
DEEP LATENT VARIABLE MODEL FOR LONGITUDINAL GROUP FACTOR ANALYSIS

Lin Qiu

The Pennsylvania State University
luq7@psu.edu

Vernon M. Chinchilli

The Pennsylvania State University
vchinch@psu.edu

Lin Lin

The Pennsylvania State University
llin@psu.edu

December 22, 2024

ABSTRACT

In many scientific problems such as video surveillance, modern genomic analysis, and clinical studies, data are often collected from diverse domains across time that exhibit time-dependent heterogeneous properties. It is important to not only integrate data from multiple sources (called multi-view data), but also to incorporate time dependency for deep understanding of the underlying system. Latent factor models are popular tools for exploring multi-view data. However, it is frequently observed that these models do not perform well for complex systems and they are not applicable to time-series data. Therefore, we propose a generative model based on variational autoencoder and recurrent neural network to infer the latent dynamic factors for multivariate time-series data. This approach allows us to identify the disentangled latent embeddings across multiple modalities while accounting for the time factor. We invoke our proposed model for analyzing three datasets on which we demonstrate the effectiveness and the interpretability of the model.

1 Introduction

Multi-view learning is an emerging problem in machine learning research, as multi-view data becomes increasingly common in many real world applications. Examples including multi-omics data where different biological layers such as genomics, epigenomics, transcriptomics and proteomics can be obtained from the same set of objects. In finance, the performance of each company may be better described in terms of different asset classes, such as stocks and bonds. In computer vision, a scene is typically represented by a series of audio and image frames. In those situations, the same set of objects typically have different features (views) collected from different measuring methods or domains, where any particular single-view data is potentially inadequate to comprehensively describe the information of all the objects. Hence, one major goal of multi-view learning is to find a lower-dimensional latent representation that can explain multiple views of the data and capture the shared variations among all views.

Many popular multi-view learning methods [1, 2, 3, 4] have been developed based on group factor analysis, which generates a common linear mapping between the latent and observed groups of variables (multiple views). In order to further extract interpretable information, most of the methods exploit the idea of using sparse linear factor models. In particular, the resulting latent factor is restricted to contribute to variation in only a subset of the observed features. For example, sparse factor loadings in gene expression data analysis can be interpreted as non-disjoint clusters of co-regulated genes [5, 6, 7]. In multi-omics studies, the sparse group factor analysis model helps to infer a set of hidden factors that capture both the biological and technical sources of variability. This information is important for downstream analysis, such as identification of sample subgroups, data imputation, and outlier sample detection [8].

Despite the wide applications of group factor analysis, existing modeling approaches are severely challenged by complex data encountered in many research areas. For example, in various disease studies, the ability to integrate different data types (e.g., genomic, transcriptomic, epigenomic, and proteomic data) obtained from both healthy and disease individuals across different time point is crucial for the understanding of disease progression which can further contribute towards translational research for personalized medicine. Existing group factor analysis methods can not handle these multi-modal time-dependent complex structures efficiently [9].

Latent variable models, on the other hand, are widely used in modeling high-dimensional time-series data. The basic idea is to use the low-dimensional latent variables to automatically induce dependency among the observed data space. Among them, the linear dynamical system [10] and hidden Markov models [11] are widely studied. However, those methods do not scale well with complex non-linear dynamics. Recently, recurrent neural networks (RNNs) [12, 13, 14, 15] display good performance in modeling sequence data, where the latent random variables in RNN function are served as “memory” of the past sequence. RNN can be further extended to integrate the dependencies between the latent random variables at neighboring timesteps, called variational recurrent neural network (VRNN) [16], which can handle complex non-linear highly structured sequential data, in the context of variational autoencoder [17].

Our motivation lies in the study of high-dimensional temporal multi-view data. We seek to infer trajectories of latent variables that provide insight into the latent, lower-dimensional structure derived from the dynamics of observed data space. Motivated by the success of VRNN for modeling temporal sequence data, we propose a new modeling strategy that integrates VRNN into the sparse group factor analysis, the resulting model can serve as a nonlinear factor model for multi-view data observed across time. Further, the model interpretability is achieved through the use of sparse priors on the latent-to-observed mappings. Specifically, each view has a generator neural network and only a small number of correlated views will be affected by each latent dimension. We label this model as deep latent variable model for longitudinal group factor analysis (DLGFA).

We evaluate the performance of proposed DLGFA on simulation, motion capture and metabolites datasets. We demonstrate the interpretability of the dynamic learned representations and how these structures of sequential interactions correspond to physically meaningful insight. We also demonstrate the model’s generative and generalization ability through the use of limited training datasets which may not fully capture the structure of interest space.

2 Related Work

In generative models, the class of variational autoencoders (VAEs) are popular for efficient approximate inference and learning [17]. VAE approximates intractable posterior distributions over latent representations that are parameterized by a deep neural network, which maps observations to a distribution over latent variables.

For non-sequential data, VAE has become one of the most popular approaches for efficiently recover complex multimodal distributions. Recently, VAE has been extended to dynamic systems [18]. Briefly, VAE provides a mapping from the observations to a distribution on their latent representation. The resulting simpler latent subspace can be used to describe the underlying complex system. Mathematically, let $\mathbf{x} \in \mathcal{R}^d$ denote a d -dimensional observation and $\mathbf{z} \in \mathcal{R}^K$ denote a vector of *latent random variables* of fixed dimension K . The generative process of VAE can be represented as: $\mathbf{z} \sim \mathcal{N}(0, I)$, $\mathbf{x} \sim \mathcal{N}(\boldsymbol{\mu}_{\mathbf{x}}, D)$, where I is the identify matrix, D is a $d \times d$ diagonal matrix whose diagonals are the marginal variances of each component of \mathbf{x} , $\boldsymbol{\mu}_{\mathbf{x}}$ is the mean of the Gaussian likelihood and is produced by a neural network with parameters θ taking \mathbf{z} as an input. As an example of a directed graphical model, the joint distribution is defined as:

$$p(\mathbf{x}, \mathbf{z}) = p(\mathbf{x} | \mathbf{z})p(\mathbf{z}) \quad (1)$$

While latent random variable models of the form given in Eq. (1) are not uncommon, endowing the conditional $p(\mathbf{x} | \mathbf{z})$ as a potentially highly non-linear mapping from \mathbf{z} to \mathbf{x} is a rather unique feature of the VAE.

The likelihood is then parameterized with a generative network (called decoder). VAE uses $q(\mathbf{z}|\mathbf{x})$ with an inference network (called encoder) to approximate the posterior distribution of \mathbf{z} . For example, $q(\mathbf{z}|\mathbf{x})$ can be a Gaussian $\mathcal{N}(\boldsymbol{\mu}, \sigma^2 I)$, where both $\boldsymbol{\mu}$ and σ^2 are parameterized by neural network: $[\boldsymbol{\mu}, \log \sigma^2] = f_{\phi}(\mathbf{x})$, where f_{ϕ} is a neural network with parameters ϕ . The parameters for both generative and inference networks are learned through variational inference, by maximizing the evidence lower bound (ELBO): $\log p(\mathbf{x}) \geq E_{q_{\phi}(\mathbf{z}|\mathbf{x})}[\log_{\theta} p(\mathbf{x}, \mathbf{z}) - \log q_{\phi}(\mathbf{z}|\mathbf{x})]$.

Output interpretable VAE (oi-VAE) extends VAE when \mathbf{x} contains a group of G features (or views) [9]. Rewrite $\mathbf{x} = [\mathbf{x}^{(1)}, \dots, \mathbf{x}^{(G)}]$ for each of the G groups. oi-VAE models each $\mathbf{x}^{(g)}$, $g \in 1 : G$ separately, while the latent variable \mathbf{z} is shared across all groups to facilitate the interpretable output. Specifically, $\mathbf{z} \sim \mathcal{N}(0, I)$, $\mathbf{x}^{(g)} \sim \mathcal{N}(\boldsymbol{\mu}_{\mathbf{x}}^{(g)}, D^{(g)})$, where $\boldsymbol{\mu}_{\mathbf{x}}^{(g)}$ and $D^{(g)}$ are the group-specific mean and diagonal covariance containing sample variances. Different from the standard VAEs, a new set of latent-to-group matrices $W^{(g)} \in \mathcal{R}^{p \times K}$ are introduced. Both $W^{(g)}$ and \mathbf{z} together determines the value of $\boldsymbol{\mu}_{\mathbf{x}}^{(g)}$: $[\boldsymbol{\mu}_{\mathbf{x}}^{(g)}] = f_{\theta_g}^{(g)}(W^{(g)} \mathbf{z})$, where $f_{\theta_g}^{(g)}$ denote a neural network with input dimension p and parameters θ_g . The idea is that the j th latent dimension \mathbf{z}_j has no influence on group g through $f_{\theta_g}^{(g)}$ if the j th column of $W^{(g)}$, $W_{\cdot, j}^{(g)}$, are all zeros. A column-wise sparsity inducing prior [19] is thus employed for $W_{\cdot, j}^{(g)}$: $\gamma_{g, j}^2 \sim \text{Ga}((p+1)/2, \lambda^2/2)$; $W_{\cdot, j}^{(g)} \sim \mathcal{N}(0, \gamma_{g, j}^2 I)$, where $\text{Ga}(\cdot, \cdot)$ is the Gamma distribution defined by shape and rate.

Larger value of λ encourages more column-wise sparsity in $W^{(g)}$. In addition, a common prior is placed for θ_g of each generator: $\theta_g \sim \mathcal{N}(0, I)$. This is to mitigate the rescaling behavior of the parameters across layer boundaries [20]. $W^{(g)}$ with very small weights may be very large in a subsequent layer that offset the sparsity effect from the prior. oi-VAE is learned through collapsed variational inference. oi-VAE is designed only for analyzing non-temporal multi-view data.

Our focus is in extending VRNN for modeling the latent variable to achieve dynamic latent representations through deep neural network for better interpretability, as in linear factor analysis.

3 Deep Latent Variable Model for Longitudinal Group Factor Analysis

Inspired by the success of the above latent random variable models, we propose to develop a novel variational recurrent model for multi-view longitudinal data analysis while achieving better interpretability as in factor analysis.

3.1 Model

Prior Given a temporal sequence of vectors $\mathbf{x}_{1:T} = (\mathbf{x}_1, \dots, \mathbf{x}_T)$, $\mathbf{x}_t \in \mathcal{R}^d$, RNN generates a set of hidden units $\mathbf{h}_t \in \mathcal{R}^p$, $t \in 1 : T$. Similar to VRNN, the latent variable \mathbf{z}_t is designed to guide the generation of \mathbf{h}_t and \mathbf{x}_t at timestep t . Hence, different from the conventional VAEs, the prior for \mathbf{z}_t is assumed to follow the distribution:

$$\mathbf{z}_t \sim \mathcal{N}(\mu_{0,t}, \text{diag}(\sigma_{0,t}^2)) \quad (2)$$

$$[\mu_{0,t}, \sigma_{0,t}] = \varphi_{\tau}^{\text{prior}}(\mathbf{h}_{t-1}) \quad (3)$$

where both $\mu_{0,t}$ and $\sigma_{0,t}$ are produced by a distinct neural network that approximates the time dependent prior distribution[16]. $[\mu_{0,t}, \log(\sigma_{0,t}^2)] = \varphi_{\tau}^{\text{prior}}(\mathbf{h}_{t-1})$, and $\varphi_{\tau}^{\text{prior}}(\mathbf{h}_{t-1})$ denote a neural network taking the previous hidden state \mathbf{h}_{t-1} as input.

Decoder Rewrite the sequence data to incorporate the group information as $\mathbf{x}_{1:T} = (\mathbf{x}_1, \dots, \mathbf{x}_T)$, $\mathbf{x}_t = [\mathbf{x}_t^{(1)}, \dots, \mathbf{x}_t^{(G)}] \in \mathcal{R}^{d \times G}$. The generation of \mathbf{x}_t will depend on both \mathbf{z}_t and \mathbf{h}_{t-1} . In addition, we propose to model different views of data independently while allowing the latent variable \mathbf{z}_t to be shared across G views at timestep t . The corresponding generative distribution will be:

$$\mathbf{x}_t^{(g)} | \mathbf{z}_t \sim \mathcal{N}(\boldsymbol{\mu}_{\mathbf{x},t}^{(g)}, D_{\mathbf{x},t}^{(g)}) \quad (4)$$

where $D_{\mathbf{x},t}^{(g)}$ is a diagonal matrix. Different from oi-VAE, we propose to introduce a sequence of latent matrices $W_t^{(g)} \in \mathcal{R}^{p \times K}$, for $t = 1 : T, g = 1 : G$. Both parameters $\boldsymbol{\mu}_{\mathbf{x},t}^{(g)}$ and $D_{\mathbf{x},t}^{(g)}$ will be conditioned on $W_t^{(g)}$, \mathbf{z}_t and \mathbf{h}_{t-1} through:

$$[\boldsymbol{\mu}_{\mathbf{x},t}^{(g)}, \log(\text{diag}(D_{\mathbf{x},t}^{(g)}))] = \varphi_{\theta_{t,g}}^{\text{dec}}(W_t^{(g)} \mathbf{z}_t, \mathbf{h}_{t-1}) \quad (5)$$

where $\varphi_{\theta_{t,g}}^{\text{dec}}$ denotes a neural network with parameters $\theta_{t,g}$, $\text{diag}(D)$ denotes the diagonal elements of the matrix D . A column-wise sparsity prior can also be placed for $W_t^{(g)}$ to ensure the interpretability of the model: $\gamma_{gjt}^2 \sim \text{Ga}((p+1)/2, \lambda^2/2)$; $W_{t,j}^{(g)} \sim \mathcal{N}(0, \gamma_{gjt}^2 I)$, Hence, the model automatically tracks the importance of \mathbf{z}_t through time.

Recurrence The hidden state \mathbf{h}_t is updated conditioning on \mathbf{z}_t in a recurrent way: $\mathbf{h}_t = S_{\theta}(\mathbf{x}_t, \mathbf{z}_t, \mathbf{h}_{t-1})$, where S is the transition function which can be implemented with gated activation functions such as long short-term memory or gated recurrent unit [21, 22]. VRNN demonstrates that by including feature extractors in the recurrent equation are important for learning complex data:

$$\mathbf{h}_t = S_{\theta}(\varphi_{\tau}^{\mathbf{x}}(\mathbf{x}_t), \varphi_{\tau}^{\mathbf{z}}(\mathbf{z}_t), \mathbf{h}_{t-1}) \quad (6)$$

where $\varphi_{\tau}^{\mathbf{x}}$ and $\varphi_{\tau}^{\mathbf{z}}$ are two neural networks for feature extraction from \mathbf{x}_t and \mathbf{z}_t , respectively. By the above model specifications, the generative distribution can be factorized as:

$$p(\mathbf{x}_{\leq T}, \mathbf{z}_{\leq T}) = \prod_{t=1}^T \left[\prod_{g=1}^G p(\mathbf{x}_t^{(g)} | \mathbf{z}_{\leq t}, \mathbf{x}_{<t}^{(g)}) \right] p(\mathbf{z}_t | \mathbf{x}_{<t}, \mathbf{z}_{<t}) \quad (7)$$

Encoder Similar to the other latent random variable models, we need to define an approximate posterior $q(\mathbf{z}|\mathbf{x})$. We let $q(\mathbf{z}|\mathbf{x})$ as a function of both \mathbf{x}_t and \mathbf{h}_{t-1} as:

$$\mathbf{z}_t|\mathbf{x}_t \sim \mathcal{N}(\boldsymbol{\mu}_{\mathbf{z},t}, D_{\mathbf{z},t})[\boldsymbol{\mu}_{\mathbf{z},t}] \quad (8)$$

$$\log(\text{diag}(D_{\mathbf{z},t})) = \varphi_{\tau}^{\text{enc}}(\varphi_{\tau}^{\mathbf{x}}(\mathbf{x}_t), \mathbf{h}_{t-1}) \quad (9)$$

The model structure is depicted in Figure 1.

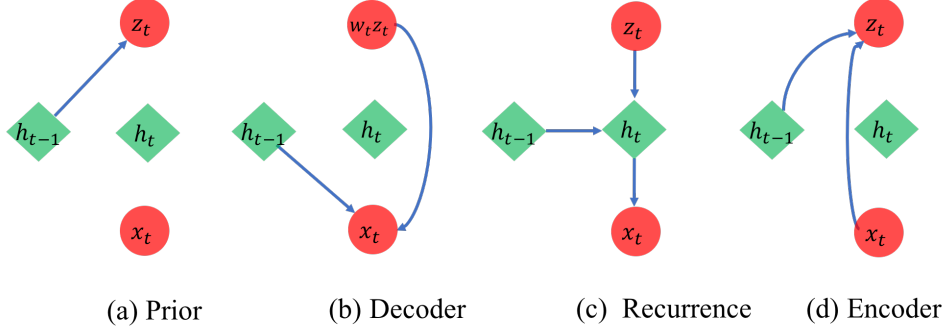


Figure 1: Graphical illustration of each operation in DLGFA model, green color represents the hidden state and red color represents data and latent variable : (a) Computing the conditional prior using Eq. (2) and (3); (b) Generating function using Eq. (4) and (5); (c) Updating RNN hidden state using Eq. (6); (d) Inference of the approximate posterior using Eq. (8) and (9).

3.2 Variational Inference

The simple approach to optimize the variational distribution can not generate true sparsity for the parameters having sparsity-inducing priors. Hence, we propose to adapt the idea of collapsed variational inference [9] to obtain true sparsity.

Let $\mathcal{W} = (\mathbf{W}_{1:T}^{(1)}, \dots, \mathbf{W}_{1:T}^{(G)})$, $\gamma^2 = (\gamma_{1:G,1:K,1:T}^2)$, $\mathbf{x} = \mathbf{x}_{1:T}$, and $\mathbf{z} = \mathbf{z}_{1:T}$. Thus, we can compute $\log p(\mathbf{x})$ by marginalizing out all γ_{gjt}^2 's:

$$\begin{aligned} \log p(\mathbf{x}) &= \log \int p(\mathbf{x}|\mathbf{z}, \mathcal{W}, \theta) p(\mathbf{z}) p(\mathcal{W}|\gamma^2) p(\gamma^2) p(\theta) d\gamma^2 dz \\ &= \log \int \left(\int p(\mathcal{W}, \gamma^2) d\gamma^2 \right) \frac{p(\mathbf{x}|\mathbf{z}, \mathcal{W}, \theta) p(\mathbf{z}) p(\theta)}{q_{\phi}(\mathbf{z}|\mathbf{x})/q_{\phi}(\mathbf{z}|\mathbf{x})} dz \\ &\geq \mathbb{E}_{q_{\phi}(\mathbf{z}_{\leq T}|\mathbf{x}_{\leq T})} \left[\sum_{t=1}^T (-\text{KL}(q_{\phi}(\mathbf{z}_t | \mathbf{x}_{\leq t}, \mathbf{z}_{<t}) || p(\mathbf{z}_t | \mathbf{x}_{\leq t}, \mathbf{z}_{<t})) + \log p(\mathbf{x}_t | \mathbf{z}_{\leq t}, \mathbf{x}_{<t})) \right] \\ &\quad + \log p(\theta_t) - \lambda \sum_{t=1}^T \sum_{g,j} \|\mathbf{W}_{\cdot,j}^{(gt)}\|_2 \end{aligned}$$

The goal is to maximize this collapsed ELBO over ϕ, θ , and \mathcal{W} . The columns of the latent-to-group matrices $\mathbf{W}_{t,j}^{(g)}$ appear in a 2-norm penalty in the new collapsed ELBO which is a group lasso penalty on the columns of $\mathbf{W}_{t,j}^{(g)}$ and encourages the entire vector to be set to zero. We propose the use of efficient proximal gradient descent updates on the latent-to-group matrices \mathcal{W} as detailed in Sec. 3.3. We can use any other optimization method, such as Adam for the remaining neural net parameters, θ and ϕ .

Algorithm 1 Collapsed VI for DLGFA

Input: data $\mathbf{x}^{(i)}$, sparsity parameter λ
Let $\tilde{\mathcal{L}}_t$ be $\mathcal{L}(\phi_t, \theta_t, \mathcal{W}_t)$ but without $-\lambda \sum_{g,j} \|\mathbf{W}_{t,j}^{(g)}\|_2$.
repeat
 For each time point t
 Calculate $\nabla_{\phi_t} \tilde{\mathcal{L}}_t$, $\nabla_{\theta_t} \tilde{\mathcal{L}}_t$, and $\nabla_{\mathcal{W}_t} \tilde{\mathcal{L}}_t$.
 Update ϕ_t and θ_t with Adam optimizer.
 Let $\mathcal{W}_{t+1} = \mathcal{W}_t - \eta \nabla_{\mathcal{W}_t} \tilde{\mathcal{L}}_t$.
 for all groups $g, j = 1$ **to** K **do**
 Set $\mathbf{W}_{t,j}^{(g)} \leftarrow \frac{\mathbf{W}_{t,j}^{(g)}}{\|\mathbf{W}_{t,j}^{(g)}\|_2} \left(\|\mathbf{W}_{t,j}^{(g)}\|_2 - \eta \lambda \right)_+$
 end for
until convergence in both $\sum_{t=1}^T \tilde{\mathcal{L}}_t$ and $-\lambda \sum_{t=1}^T \sum_{g,j} \|\mathbf{W}_{t,j}^{(g)}\|_2$

3.3 Proximal Gradient Descent

A *proximal algorithm* is an algorithm for solving a convex optimization problem which uses the proximal operators of the objective terms. Consider the problem

$$\min_x f(x) + g(x), \quad (10)$$

where $f : \mathbf{R}^n \rightarrow \mathbf{R}$ and $g : \mathbf{R}^n \rightarrow \mathbf{R} \cup \{+\infty\}$ are closed proper convex and f is differentiable [23].

The proximal gradient method is

$$x^{k+1} = \text{prox}_{\lambda^k g}(x^k - \lambda^k \nabla f(x^k)), \quad (11)$$

where $\lambda^k > 0$ is a step size, $\text{prox}_f(x)$ is the proximal operator for the function f . Expanding the definition of $\text{prox}_{\lambda^k g}$, we can show that the proximal step corresponds to minimizing $g(x)$ plus a quadratic approximation to $g(x)$ centered on x^k . For $g(x) = \eta \|x\|_2$, the proximal operator is given by

$$\text{prox}_{\lambda^k g}(x) = \frac{x}{\|x\|_2} \left(\|x\|_2 - \lambda^k \eta \right)_+ \quad (12)$$

According to Parikh and Boyd (2014), we know $(v)_+ \triangleq \max(0, v)$. This operator can reduce x by $\lambda \eta$, and x can be shrunk to zero under $\|x\|_2 \leq \lambda^k \eta$. Ainsworth et al. (2018) used proximal stochastic gradient updates for \mathcal{W} and found that collapsed variational inference with proximal updates can not only provided faster convergence but also achieved model sparsity, we adapted this approach to update each time point of \mathcal{W} .

4 Model Interpretation

Dynamic latent embeddings DLGFA builds on VRNN for longitudinal multi-view data. By mapping each of the latent components in \mathbf{z} to a subset of the groups at different time points, we can identify the disentangled representations in the latent space and study its variations in a time manner. To make the latent embeddings interpretable, DLGFA generates sparse latent-to-group matrix \mathcal{W} so that: (1) For the latent components that are only specific to a particular group at time t , these components are allowed to explain the variation only to the individual group, and are independent of all the other groups. This is achieved through the fact that there will be only one $\mathbf{W}_t^{(g)} \neq 0$. (2) For the remaining components which are not group-specific at time t , their values are non-zero if they are responsible for describing the relationships among some groups, and zero for the others. These two properties are achieved by the sparsity prior on \mathcal{W} . Each dimension of \mathbf{z} will capture the distinct modes of variation. For example, Table 1 shows that at different time points, the learned latent components on human motion capture recordings associated with only a subset of the joints (groups) that related to walking.

Dynamic group interactions Since each latent component can only be associated with a subset of groups, the relationship between the dimension of \mathbf{z} and the groups can be used as a exploratory tool to indicate the dependency among different groups. DLGFA is appealing for this since most of the complex systems depend on a temporal component, which drives variable interactions to evolve consistently during its extent. By accessing the dynamic relationship of groups of variables will help us gain insight for downstream analysis of the complex data. For example,

in environmental perturbation studies, the biological system will respond to the stress in a very fast way and make physiology adjustment properly on the cellular and molecular level. The stress response will trigger a series of repairing strategies like catalase during oxidative stress, protein chaperones under temperature stress, and other general responses which could result in down regulation of genes expression [24].

5 Experiment

5.1 Artificial Data

In order to visualize the performance of DLGFA, we generate 2000 8×8 images, where each row in the image corresponds to one view (group). For each image, we first randomly select one row to assign non-zero values, and the rest having zero values. Next, we add normal random noises with mean 0 and standard deviation 0.05 to the entire image. A particular generated image is illustrated in Figure 2 (a), where yellow colors correspond to non-zero values, and dark blue means zero value. To induce dependencies among the images, we randomly select 64 images for each batch from 2000 images and then replicate each image 32 times from those selected 64 images to represent the perfect dependent time series structure. For each batch, the data structure is of $32 \times 64 \times 8 \times 8$. In order to associate each dimension of \mathbf{z} with a unique row in the image, we chose $K = 8$. Results are shown in Figure 2. First, Figure 2 (b) shows that DLGFA can accurately reconstruct the original image, where the reconstructed image is obtained through generative net(decoder). Second, Figure 2 (c) shows that DLGFA can also successfully disentangle each of the dimensions of \mathbf{z} to correspond to exactly one row (group) of the image at each time point. We also tried different values of λ , and based on the results shown in Figure 2 (c) and (d), we choose $\lambda = 5$ for the rest of the experiments. We also tried larger values of λ is the rest of the analyses, we do not observe any significant differences.

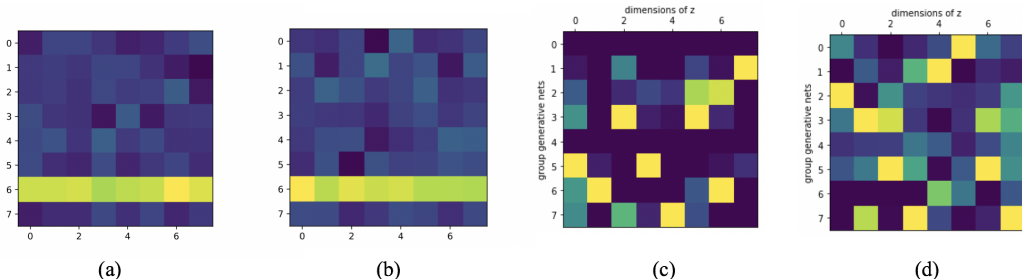


Figure 2: DLGFA results on Artificial data. (a) A particular generated image; (b) DLGFA reconstruction to the image in (a); (c) Learned DLGFA $\mathbf{W}_{t,j}^{(g)}$ at time point 10 for $\lambda = 5$ and (d) $\lambda = 1$.

5.2 Motion Capture

In this section, we use the motion capture data obtained from CMU (<http://mocap.cs.cmu.edu>) to evaluate DLGFA’s ability to handle complex time series multi-view data. This dataset contains 11 trails of standard walking and one brisk walking recordings from the same person. For each trail, it contains different time frames of the person’s moving skeleton, and it measures 59 joint angles split across 29 distinct joints. In this study, we can treat each distinct joint as a view (group), and each joint has 1 to 3 observed degrees of freedom to represent the different group dimensions. For model training, we use the data from 1 to 10 trails and $T = 32$ frames. We evaluate our experiments on: (1) The learned dynamic latent components and its interpretability for the view interactions; (2) The generative ability to capture the hidden dynamics information; (3)The test-loglikelihood to assess model generalization ability.

To check different latent dimensions’ effect of \mathbf{z} , we train DLGFA on $K = 4, 8, 16$. Figure 3 shows the results for $K = 8$. Results for the other values of K are in supplementary material. Figure 3 shows that the factors change across different time points. For example, from time point 1 to 3, the first factor (first column of the left and middle images) changes from lfoot (left foot) to rfoot (right foot), factor 2 changes from rwrist (right wrist) to thorax, and factor 7 changes from rwrist to rtibia (right tibia). These changes are indeed reasonable since when we start to walk with foot, tibia and thorax move accordingly [25]. The above observation demonstrates that the learned latent representation from DLGFA has an intuitive anatomical interpretation for different time points. We also provided a detailed list of the joints per latent variable dimension that are most strongly influenced by each factor in Table 1. For example, factor 1 represents foot and lower back, factor 2 represents wrist,thorax and upper back, and factor 8 represents wrist, foot and

Table 1: Top joints corresponding to each latent dimension determined by $\mathbf{W}_{:,j}^{(g)}$.

DIM	$t=1$	$t=3$	$t=7$
1	LFOOT	RFOOT	LOWERBACK
2	RWRIST	THORAX	UPPERBACK
3	LOWERNECK	LTHUMB	UPPERBACK
4	HEAD	RFOOT	LFEMUR
5	THORAX	HEAD	RFEMUR
6	LHAND	LFOOT	LFOOT
7	RHUMERUS	HEAD	UPPERNECK
8	RFEMUR	RTIBIA	
	RWRIST	LFOOT	LHAND

hand. All these observations demonstrate that DLGFA can track the dynamic latent embeddings and provide meaningful interpretation.

To evaluate the generative ability of DLGFA, we show the reconstructed images of trail 1 for 7 time points in Figure 4 top row. The hidden dynamic information extracted from DLGFA generates very natural poses of human walking. In fact, there is clearly a moving pattern from the head to foot between neighboring timesteps. On the other hand, the results obtained from oi-VAE, which treats each time frame data independently, are very similar among each other, except the last timestep $t = 20$.

To further evaluate DLGFA’s generalization ability, we train both oi-VAE and DLGFA on trail 1 to 10, and test the model performance on trail 11, which is the standard walking data. Figure 5 shows the reconstructed images obtained from both models and the true images. Compared with oi-VAE, the images generated by DLGFA have a natural trend of walking with respect to the foot pose. We further compare the test-loglikelihood on trail 11 and trail 12, which is the brisk walk data. Table 2 records the log-likelihood for both DLGFA and oi-VAE models on two testing trails with $K = 4, 8$. DLGFA has higher test log-likelihood and both methods achieve higher test log-likelihood when the latent dimension K is larger. This indicates that DLGFA can achieve better generalization, because the brisk walking trail is very different from the training walking trails.

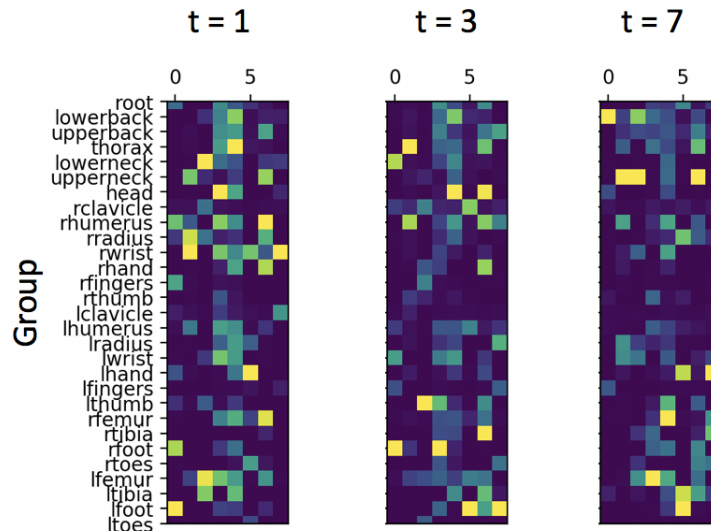


Figure 3: DLGFA results for motion capture data with $K = 8$ for three selected time points $t = 1, 3, 7$. Each row corresponds to each group of the joints, columns represent different latent dimensions. Specifically, the values of latent dimensions are color-coded from dark blue (zero) to yellow (maximum non-zero value) to indicate the strength of the latent-to-group mappings $\mathbf{W}_{t,j}^{(g)}$.

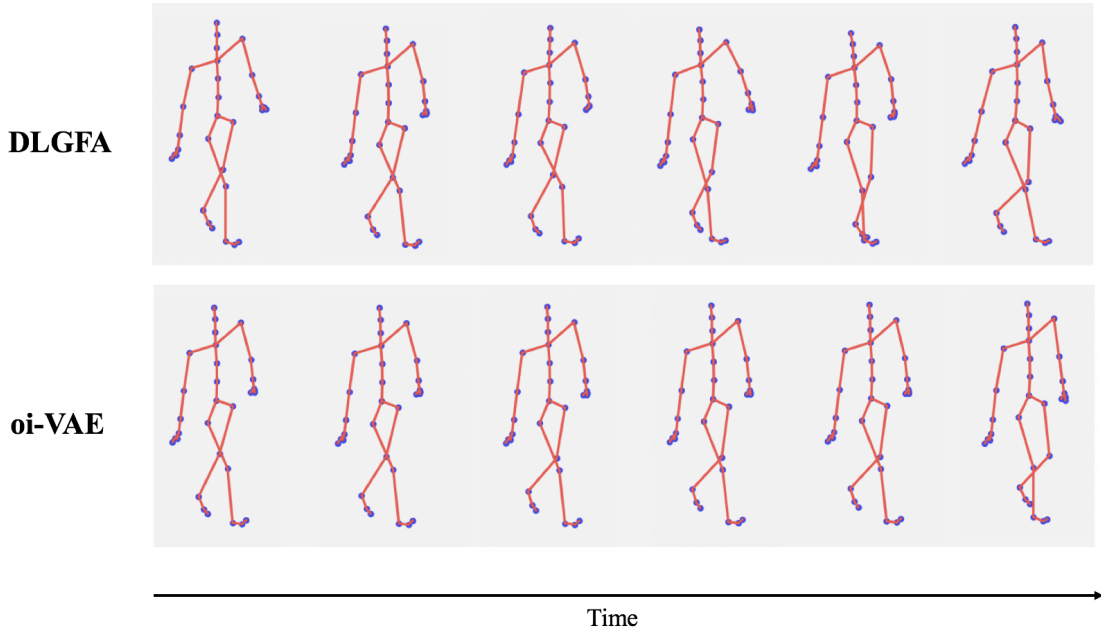


Figure 4: DLGFA (top row) and oi-VAE (bottom row) reconstructed images. Both models are trained on the first 10 trail walking data. The generated images are from trail 1 at time point $t = 1, 3, 5, 7, 9, 20$.

Table 2: Test log-likelihood for DLGFA and oi-VAE trained on the first 10 trails of walking data. Table includes results for a test walk (similar as training) and the brisk walk trial (different from training).

	STANDARD WALK	BRISK WALK
DLGFA(K=4)	-93, 221	-30, 056
oi-VAE(K=4)	-1,006,120	-598,660
DLGFA(K=8)	-17, 667	-36, 299
oi-VAE(K=8)	-998,849	-492,411

5.3 Metabolomic Data

Environmental fluctuations have led to a fast and appropriate adjustment of the physiology of *Escherichia coli* (*E.coli*) on every level of the cellular and molecular network. *E.coli* has been intensively investigated because of the efficiency in its system response to perturbation [26, 27, 24]. In this section, we propose to re-analyze the data obtained from a longitudinal study [24], where one of the objectives is to compare metabolic changes of *E.coli* response to five different perturbations: cold, heat, oxidative stress, lactose diauxie, and stationary phase. The original paper conducted multiple t-tests between neighboring time points and across different perturbations to identify the number of significant changes on metabolites.

The dataset contains 196 metabolite expression values at 12 different time points under five stress conditions. We treat each condition as a group and apply DLGFA with $\lambda = 5$ and run algorithm 1 for 10,000 iterations. Since we propose to compare our results with the group factor analysis (<https://github.com/cran/GFA>), where the algorithm automatically chose $K = 30$ as the optimum dimension. We, therefore, use $K = 30$ for DLGFA in order to obtain proper comparison. The learned group-weights $\|W_{t,j}^{(g)}\|_2$ from DLGFA and GFA are showed in Figure 6. For DLGFA, it is clear that at time $t = 3$, most of the factors' variations are explained by cold and heat groups, at time $t = 5$, cold and lactose group explain most of the variations and at time $t = 8$, lactose dominates most of the variation. These results are consistent with the findings in the original paper [24], which shows that lactose shift results in the largest number of significant value changes of metabolites after stress followed by cold stress, oxidative stress and heat stress, and no significant changes were observed for the control cultures. Meanwhile, the growth curve of *E.coli* under lactose shift after perturbation is much sharper during the late time stage compared to all other conditions in their paper, which is also quite obvious at $t = 8$ in our results. On the other hand, group factor analysis results in different findings. In

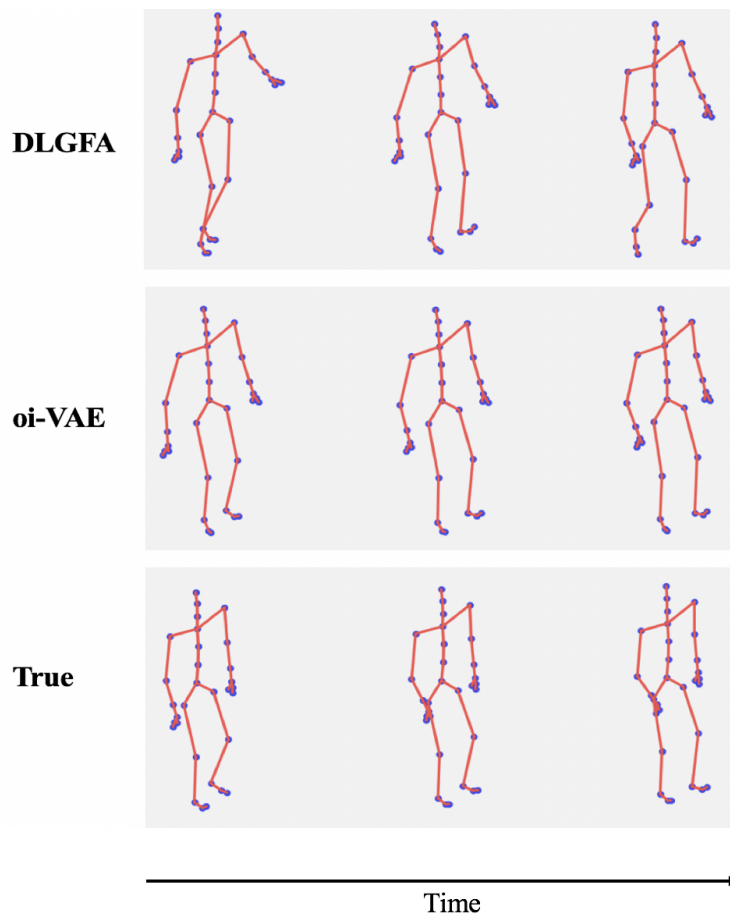


Figure 5: Reconstructed images of trail 11 at time point $t = 3, 5, 7$.

particular, at $t = 3$, oxidative condition explains the most variations and heat is the least. At $t = 5$, there is little difference among cold and oxidative stress, and at $t = 8$, there is little difference among control, heat and lactose. Those results indicate that the generic group factor analysis is not capable in capturing the true variations shared by groups under a complex time-series system. In addition, our model can further help in checking the dynamics for a particular factor. For example, DLGFA shows that factor 8 represents lactose shift and oxidative stress at early stage $t = 3$, but, it disappears for lactose shift in the later stage and only represents oxidative stress, which means factor 8 might be related with the lactose biogenesis pathway and can make quick physiology adjustment for such stress. Another advantage for DLGFA is that we can choose the latent dimension K , when K equal to the variable numbers in each group, by checking the loading values for each variable we will be able to identify the subset of variables in each group that account for the variations.

6 Conclusion

We have developed a nonlinear framework for longitudinal group factor analysis, namely DLGFA, with the goal of disentangling the dynamically shared latent embeddings for multiple groups (views) of data. One key feature of DLGFA is its ability to integrate the variational recurrent neural network to the shared latent variables among different groups to model the complex sequence data and extract the dependency relationships.

Our empirical analysis on both motion capture and metabolomics data demonstrates that DLGFA can successfully extract the hidden time series structures. More importantly, the achieved model efficiency and interpretability does not cost model generalization. Because DLGFA can model complex time series data and result in interpretable results,

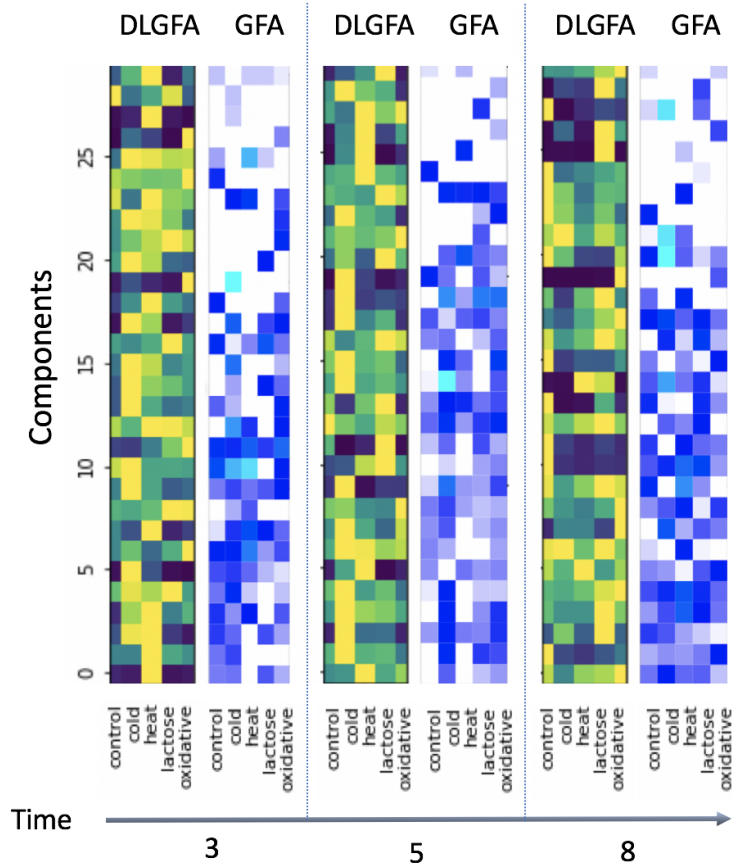


Figure 6: Results on metabolomic data. Learned $W_{.,j}^{(g)}$ at time point $t = 3, 5, 8$ under control, cold, heat, lactose shift and oxidative stress from DLGFA and GFA.

we believe DLGFA will have wide applications in different fields ranging from computer vision, disease studies, and finance.

DLGFA has the potential to be extended to accommodate different distributions and this is increasingly important in complex data, such as in clinical studies where genetic profiles, laboratory test results, and history and severity of illness are simultaneously available. To better understand the complex system, it is appealing that our model can account for both the underlying data structures and data characteristics.

References

- [1] K. Sridharan and S. M. Kakade. An information theoretic framework for multi-view learning. In *In Proceedings of COLT*, pages 403–414, 2008.
- [2] A. Klami, S. Virtanen, E. Leppaaho, and S. Kaski. Group factor analysis. *IEEE Transactions on Neural Networks and Learning Systems*, 26:2136–2147, 2015.
- [3] S. Zhao, C. Gao, S. Mukherjee, and B. E. Engelhardt. Bayesian group factor analysis with structured sparsity. *Journal of Machine Learning Research*, 17(4):1–47, 2016.
- [4] E. Leppaaho, M. Ammad-ud-din, and S. Kaski. Gfa: Exploratory analysis of multiple data sources with group factor analysis. *Journal of Machine Learning Research*, 18:1–5, 2017.
- [5] I. Pournara and L. Wernisch. Factor analysis for gene regulatory networks and transcription factor activities profiles. *BMC Bioinformatics*, 8:61, 2007.
- [6] J. E. Lucas, H. Kung, and J. A. Chi. Latent factor analysis to discover pathway-associated putative segmental aneuploidies in human cancers. *PLoS Computational Biology*, 6(9):e1000920, 2010.

- [7] C. Gao, C. D. Brown, and B. E. Engelhardt. A latent factor model with a mixture of sparse and dense factors to model gene expression data with confounding effects. *arXiv:1310.4792*, 2013.
- [8] R. Argelaguet, B. Velten, D. Arnol, S. Dietrich, T. Zenz, J. C. Marioni, F. Buettner, W. Huber, and O. Stegle. Multi-omics factor analysis—a framework for unsupervised integration of multi-omics data sets. *Molecular Systems Biology*, 14:e8124, 2018.
- [9] S. K. Ainsworth, N. J. Foti, A. K. C. Lee, and E. B. Fox. oi-vae: Output interpretable vaes for nonlinear group factor analysis. In *Proceedings of the 35th International Conference on Machine Learning (ICML 18)*, 2018.
- [10] L. Rabiner and B. Juang. An introduction to hidden markov models. *IEEE ASSP Magazine*, 3:4–16, 1986.
- [11] R. Kalman. Mathematical description of linear dynamical systems. *J. the Society for Industrial and Applied Mathematics*, Series A, 1963.
- [12] J. Martens and I. Sutskever. Learning recurrent neural networks with hessian-free optimization. In *Proceedings of the 28th International Conference on International Conference on Machine Learning (ICML 11)*, pages 1033–1040, 2011.
- [13] M. Hermans and B. Schrauwen. Training and analyzing deep recurrent neural networks. In *Proceedings of the 26th International Conference on Neural Information Processing Systems (NIPS 13)*, volume 1, pages 190–198, 2013.
- [14] R. Pascanu, T. Mikolov, and Y. Bengio. On the difficulty of training recurrent neural networks. In *Proceedings of the 30th International Conference on International Conference on Machine Learning (ICML 13)*, volume 28, pages 1310–1318, 2013.
- [15] A. Graves. Generating sequences with recurrent neural networks. *arXiv:1308.0850*, 2013.
- [16] J. Chung, K. Kastner, L. Dinh, K. Goel, and A. Courville. A recurrent latent variable model for sequential data. In *Proceedings of the 28th International Conference on Neural Information Processing Systems (NIPS 15)*, pages 2980–2988, 2015.
- [17] D. P. Kingma and M. Welling. Auto-encoding variational bayes. *arXiv:1312.6114*, 2013.
- [18] E. Archer, I. M. Park, L., J. Cunningham, and L. Paninski. Black box variational inference for state space models. In *arXiv:1511.07367*, 2015.
- [19] M. Kyung, J. Gill, and G. Casella. Penalized regression, standard errors, and bayesian lassos. *Bayesian Analysis*, 5(2):369–412, 2010.
- [20] B. Neyshabur, R. R. Salakhutdinov, and N. Srebro. Path sgd: Path-normalized optimization in deep neural networks. In *In Advances in Neural Information Processing*, pages 2422–2430, 2015.
- [21] K. Cho, B. van Merriënboer, C. Gulcehre, D. Bahdanau, F. Bougares, H. Schwenk, and Y. Bengio. Learning phrase representations using RNN encoder–decoder for statistical machine translation. In *Proceedings of the 2014 Conference on Empirical Methods in Natural Language Processing (EMNLP)*, pages 1724–1734, Doha, Qatar, October 2014. Association for Computational Linguistics.
- [22] S. Hochreiter and J. Schmidhuber. Long short-term memory. *Neural computation*, 9(8):1735–1780, 1997.
- [23] N. Parikh and S. Boyd. Proximal algorithms. *Foundations and Trends® in Optimization*, 1(3):127–239, 2014.
- [24] S. Jozefczuk, S. Klie, G. Catchpole, J. Szymanski, A. Cuadros-Inostroza, D. Steinhauser, J. Selbig, and L. Willmitzer. Metabolomic and transcriptomic stress response of escherichia coli. *Molecular Systems Biology*, 6, 2010.
- [25] M. Versichele, T. Neutens, M. Delafontaine, and N. V. D. Weghe. The use of bluetooth for analysing spatiotemporal dynamics of human movement at mass events: A case study of the ghent festivities. *Applied Geography*, 32:208–220, 2012.
- [26] M. Gadgil, V. Kapur, and W. S. Hu. Transcriptional response of escherichia coli to temperature shift. *Biotechnology Progress*, 21, 2005.
- [27] T. Durfee, A. M. Hansen, F. R. Blattner, and D. J. Jin. Transcription profiling of the stringent response in escherichia coli. *Journal of Bacteriol*, 190:1084–1096, 2008.